The Astronomical Journal, 145:2 (11pp), 2013 January doi:10.1088/0004-6256/145/1/2

2MASS J035523.37+113343.7: A YOUNG, DUSTY, NEARBY, ISOLATED BROWN DWARF RESEMBLING A GIANT EXOPLANET

Jacqueline K. Faherty[1,2], Emily L. Rice[2,3], Kelle L. Cruz[2,4], Eric E. Mamajek[5,6], and Alejandro Núñez[2,4]
[1] Department of Astronomy, Universidad de Chile Cerro Calan, Las Condes, Chile; jfaherty17@gmail.com
[2] Department of Astrophysics, American Museum of Natural History, Central Park West at 79th Street, New York, NY 10034, USA; jfaherty@amnh.org
[3] Department of Engineering Science and Physics, College of Staten Island, 2800 Victory Boulevard, Staten Island, NY 10301, USA
[4] Department of Physics and Astronomy, Hunter College, 695 Park Avenue, New York, NY 10065, USA
[5] Cerro Tololo Inter-American Observatory, Casilla 603, La Serena, Chile
[6] Department of Physics and Astronomy, University of Rochester, Rochester, NY 14627-0171, USA
Received 2012 May 13; accepted 2012 October 17; published 2012 November 20

ABSTRACT

We present parallax and proper motion measurements, near-infrared spectra, and *Wide-field Infrared Survey Explorer* photometry for the low surface gravity L5γ dwarf 2MASS J035523.37+113343.7 (2M0355). We use these data to evaluate photometric, spectral, and kinematic signatures of youth as 2M0355 is the reddest isolated L dwarf yet classified. We confirm its low-gravity spectral morphology and find a strong resemblance to the sharp triangular shaped *H*-band spectrum of the ∼10 Myr planetary-mass object 2M1207b. We find that 2M0355 is underluminous compared to a normal field L5 dwarf in the optical and Mauna Kea Observatory J, H, and K bands and transitions to being overluminous from 3 to 12 μm, indicating that enhanced photospheric dust shifts flux to longer wavelengths for young, low-gravity objects, creating a red spectral energy distribution. Investigating the near-infrared color–magnitude diagram for brown dwarfs confirms that 2M0355 is redder and underluminous compared to the known brown dwarf population, similar to the peculiarities of directly imaged exoplanets 2M1207b and HR8799bcd. We calculate *UVW* space velocities and find that the motion of 2M0355 is consistent with young disk objects (<2–3 Gyr) and it shows a high likelihood of membership in the AB Doradus association.

Key words: astrometry – brown dwarfs – stars: individual (2MASS J035523.51+113343.7) – stars: low-mass

Online-only material: color figures

1. INTRODUCTION

With masses intermediate between stars and planets (i.e., below the hydrogen burning and above the deuterium burning mass limit), brown dwarfs provide a natural link between stellar astrophysics and the planetary science of gas giants (Saumon et al. 1996; Chabrier & Baraffe 1997). Studies of the population have informed our understanding of low-mass star formation as well as the physical and chemical composition of low-temperature photospheres (e.g., Burrows et al. 2001, 1997; Chabrier et al. 2000). With an increasing number of brown dwarf discoveries, the diversity of the population in age, atmospheric properties, and chemical composition is becoming apparent.

Brown dwarfs are classified using red optical or near-infrared spectra and show characteristics which distinguish them as L ($T_{\rm eff}$ ∼ 2200–1300 K) or T/Y ($T_{\rm eff}$ < 1300) dwarfs (Kirkpatrick et al. 1999; Burgasser et al. 2002; Cushing et al. 2011; Tinney et al. 2012). The majority of spectrally classified field brown dwarfs within the literature are nearby isolated L dwarfs. Among the ∼1000 objects spanning this temperature regime, a significant portion exhibit near-infrared colors, spectral energy distributions (SEDs), and kinematics consistent with a field age population (e.g., Kirkpatrick et al. 2000; Knapp et al. 2004; Cruz et al. 2007; Chiu et al. 2006; Faherty et al. 2009; Schmidt et al. 2010). However, there are subsets exhibiting strong deviations in observational properties from the general population including low-metallicity subdwarfs, low surface gravity objects, and potentially cloudy/cloudless L dwarfs (Burgasser et al. 2003, 2007; Burgasser 2004; Looper et al. 2008; Cruz et al. 2009; Cushing et al. 2009; Kirkpatrick et al. 2010; Rice et al. 2010; Radigan et al. 2012; Gizis et al. 2012).

The most relevant sub-population to giant exoplanet studies is young (i.e., low surface gravity) isolated L dwarfs. The archetypal low surface gravity L dwarf, 2MASS J01415823−4633574 (2M0141), was discovered by Kirkpatrick et al. (2006). Its optical spectrum exhibits strong bands of VO but abnormally weak TiO, K, and Na absorption. In the near-infrared, its red $J - K_s$ color (Two Micron All Sky Survey (2MASS) $J - K_s$ = 1.73) and triangular *H*-band spectral morphology distinguish it from field L dwarfs (Kirkpatrick et al. 2010; Patience et al. 2012). It is suspected to be a member of the β Pictoris or Tucana–Horologium association, although the precise kinematics required to confirm association have not yet been determined (Kirkpatrick et al. 2010). After the discovery and characterization of 2M0141, additional isolated L dwarfs sharing similar photometric and spectral peculiarities attributed to a low surface gravity were reported (e.g., Reid et al. 2008; Cruz et al. 2009; Kirkpatrick et al. 2010). While the ages of these seemingly young L dwarfs remain largely unconstrained, there are kinematic and spatial indications that they represent the lowest mass members of nearby moving groups such as AB Doradus, β Pictoris, Tucana–Horologium (Cruz et al. 2009; Kirkpatrick et al. 2010).

Cruz et al. (2009) point out that the majority of objects defining the population of the lowest surface gravity L dwarfs show spectral deviations indicating that they are younger than the Pleiades. Therefore using an age range[7] of <10–100 Myr and spectral classifications of early–mid type L dwarfs, these objects have masses close to—or in some cases below—the deuterium burning limit, making them exoplanet analogs. Since young brown dwarfs are nearby and isolated, they are ideal laboratories for detailed studies of cool, low-gravity, dusty atmospheres that are similar to directly imaged exoplanets.

[7] 10 Myr chosen as the low-end range based on the age of the youngest nearby moving group. 100 Myr chosen as the upper limit based on an extrapolation and comparison to Pleiades age objects.

In this paper we examine the kinematic, photometric, and spectral features of the low surface gravity L5γ dwarf 2MASS J035523.37+113343.7 (2M0355). In Section 2 we review published observations of 2M0355. In Section 3 we describe new near-infrared spectral and imaging data, and in Section 4 we evaluate indications of youth, including potential membership in nearby young moving groups. In Section 5 we discuss the SED for 2M0355 as well as the near-infrared color–magnitude diagram for the brown dwarf population, highlighting the location of 2M0355 compared to directly imaged exoplanets. Conclusions are presented in Section 6.

2. PUBLISHED OBSERVATIONS OF 2M0355

2M0355 was discovered by Reid et al. (2006) in a search of the 2MASS database for ultracool dwarfs, but its observational peculiarities were not discussed until Reid et al. (2008) and Cruz et al. (2009). 2M0355 is classified as an L5γ dwarf,[8] demonstrating strong Li absorption (EW 7.0 Å) and other signatures of low surface gravity in the optical (Reid et al. 2008; Cruz et al. 2009). Notably this source is the reddest isolated L dwarf yet classified, with a 2MASS $J - K_s$ color of 2.52 ± 0.03.

Reid et al. (2006) examined 2M0355 for a close companion with the Near-Infrared Camera and Multi-Object Spectrometer NIC1 on the *Hubble Space Telescope* and found it unresolved. Blake et al. (2007) examined this source for radial velocity (RV) variations but found no appreciable change over time and excluded the possibility of a companion with $M \sin i > 2.0\ M_J$ at any separation. We note that Blake et al. (2007) assumed an L dwarf primary mass of 100 M_J, which is large for even a field aged object; therefore, given the RV constraints, the limit is likely below 2.0 $M_{\rm Jup}$. Bernat et al. (2010) claimed the detection of a near-equal-mass companion at 82.5 mas using aperture masking interferometry; however, this result falls at the low end of their confidence limits (90%) and such a companion should have been detected by the Reid et al. (2006) imaging campaign (although Bernat et al. 2010 note this object may be at the limit of Reid et al. 2006 detections).

RVs of 12.24 ± 0.18 and 11.92 ± 0.22 km s^{-1} were measured by Blake et al. (2007, 2010), respectively, using high-resolution K-band spectra from NIRSPEC on the Keck II telescope and forward modeling techniques for high precision. Proper motion measurements have been reported in Schmidt et al. (2007), Casewell et al. (2008), and Faherty et al. (2009). We present an updated proper motion as well as a parallax in Section 4.3.

3. NEW OBSERVATIONS OF 2M0355

We obtained near-infrared spectroscopy and imaging of 2M0355 and report new low- and medium-resolution spectroscopy of the source as well as a parallax and improved proper motion measurements.

3.1. Near-infrared Spectroscopy

We obtained low- and medium-resolution near-infrared spectroscopy using the SpeX spectrograph (Rayner et al. 2003) mounted on the 3 m NASA Infrared Telescope Facility (IRTF). On 2007 November 13, we used the spectrograph in cross-dispersed (SXD) mode with the 0.″5 slit aligned to the parallactic angle to obtain $R \equiv \lambda / \Delta\lambda \approx 1200$ spectral data over the wavelength range of 0.7–2.5 μm. The conditions of this run were clear and stable with seeing of 0.″5 at K. We obtained six individual exposure times of 300 s in an ABBA dither pattern along the slit.

On 2011 December 7, we used the spectrograph in prism mode with the 0.″5 slit aligned to the parallactic angle. This resulted in $R \equiv \lambda / \Delta\lambda \approx 120$ spectral data over the wavelength range of 0.7–2.5 μm. Conditions included light cirrus and the seeing was 0.″8 at K. We obtained 10 individual exposure times of 90 s in an ABBA dither pattern along the slit. Table 1 contains details on all observations reported in this work.

Immediately after the science observation we observed the A0V star HD 25175 (Prism mode) or HD 25258 (SXD mode) at a similar airmass for telluric corrections and flux calibration. Internal flat-field and Ar arc lamp exposures were acquired for pixel response and wavelength calibration, respectively. All data were reduced using the SpeXtool package version 3.4 using standard settings (Cushing et al. 2004; Vacca et al. 2003).

3.2. Near-infrared Imaging

We observed 2M0355 with the Infrared Side Port Imager (ISPI; van der Bliek et al. 2004) on the CTIO 4 m Blanco telescope six times between 2008 October 11 and 2012 February 5. All observations used the J-band filter, under seeing conditions up to 2″ FWHM with typical conditions between 0.″8 and 1.″1. ISPI has a ∼8 arcmin field of view and plate scale of 0.″303 pixel^{-1}. At each epoch and depending on the conditions, 5–10 images with 10–30 s and 2–4 co-adds were obtained while the target was ±30 minutes off the meridian (Table 1). Dark frames and lights on/off dome flats were obtained at the start of each evening. We used the Carnegie Astrometric Planet Search software to extract all point sources from each epoch and solve for relative parallaxes and proper motions (Boss et al. 2009). The full image reduction procedures as well as the description of the parallax pipeline are described in Faherty et al. (2012).

4. EVALUATING YOUTH INDICATORS

Youth indicators for isolated L dwarfs are not yet fully quantified or calibrated, but a number of distinguishing characteristics have been extrapolated from low-mass members (primarily late-type M dwarfs) of nearby young moving groups, open clusters, and star-forming regions or companions to young stars and confirmed by low-gravity atmosphere models (e.g., Lucas et al. 2001; Gorlova et al. 2003; Luhman et al. 2004; McGovern et al. 2004; Allers et al. 2007; Rice et al. 2010, 2011; Patience et al. 2012).

Among the strongest indicators is the shape of the near-infrared spectra of young brown dwarfs, which are subtly different than those of their field counterparts. Known brown dwarf members of the Chamaeleon II, Ophiuchus, Orion Nebula Cluster, TW Hydrae, and β Pictoris groups demonstrate various degrees of sharply peaked H-band spectra compared to field aged objects. The shape of the near-infrared continuum induced by steam absorption is sensitive to an objects surface gravity; therefore at younger ages, hence lower gravities, the H-band spectrum is peaked (Luhman et al. 2004 and Figure 6 from Rice et al. 2011).

An equally important indicator for brown dwarf members of young groups is a strong deviation in near-infrared color (significantly redder $J - K_s$) from the mean of a given spectral subtype. The clearest example is 2MASS J12073346−3932539

[8] As suggested by Kirkpatrick (2005), Kirkpatrick et al. (2006), and Cruz et al. (2009), very-low-gravity spectra are designated with subtype γ, intermediate gravity with β, and normal field objects with α (although α is typically omitted/implied for field objects.

Table 1
Near-infrared Observations

Telescope	Instrument	Exp. Time × Co-adds (s)	Images	Date	Airmass	Filter/Mode
(1)	(2)	(3)	(4)	(5)	(6)	
CTIO 4M	ISPI	30 × 2	5	2008 Oct 11	1.3	*J*
		10 × 4	5	2008 Dec 12	1.3	*J*
		10 × 4	5	2009 Nov 30	1.3	*J*
		10 × 4	5	2010 Jan 28	1.5	*J*
		30 × 4	10	2011 Nov 11	1.3	*J*
		30 × 2	10	2012 Jan 3	1.3	*J*
		30 × 4	5	2012 Feb 5	1.4	*J*
IRTF	SpeX	90 × 1	10	2011 Dec 7	1.2	Prism
	SpeX	300 × 1	6	2007 Nov 13	1.0	SXD

(2M1207b), a late-L dwarf member of the TW Hydrae association with $J-K = 3.05$, ~0.5 mag redder than any other known L dwarf (Chauvin et al. 2004; Mohanty et al. 2007). Similar to the spectral deviations of young brown dwarfs, the photometric peculiarities can be explained as a consequence of lower surface gravity. At lower values—hence lower pressure at a given temperature in the photosphere—H_2 collision-induced absorption (CIA) is reduced leading to a reduction of the strongest absorption feature at 2.5 μm (less absorption at *K* band relative to *J* band) and a red $J-K$ color (Kirkpatrick et al. 2006). An evolutionary model comparison of a large collection of low surface gravity or young companion brown dwarfs to tracks with differing cloud, metallicity, and gravity properties demonstrates that the change in near-IR color is attributed to changes in CIA H_2 affected by lower surface gravities (see Faherty et al. 2012 and references therein).

Additionally, the kinematics of young brown dwarfs as a population can be used as an indicator of youth as they are distinctly different from the kinematics of the field brown dwarf population. As discussed in Faherty et al. (2009, 2012) low surface gravity brown dwarfs have significantly smaller tangential velocities and dispersions than the overall brown dwarf population. The young age (likely <1 Gyr) of these sources means they have spent less time in the disk so they have had minimal interactions with nearby stars and giant molecular clouds that will eventually increase their overall velocity dispersion (e.g., Weinberg et al. 1987; Faherty et al. 2010; Dhital et al. 2010).

In the following subsections we compare the photometry, near-infrared spectral features, and kinematics of 2M0355 to known young brown dwarfs, directly imaged exoplanets, and the field population in order to evaluate signatures of youth for this unusual object.

4.1. Photometry

2M0355 is the reddest isolated L dwarf known. In Figure 1 we show the mean $J - K_s$ color and standard deviation for L dwarfs (binned by 0.5 subtype) calculated from a compilation of field objects[9] with photometric uncertainties <0.1, excluding known young objects and subdwarfs. For comparison, other confirmed low-gravity Lγ dwarfs are plotted as filled circles and 2M0355 as a filled five-point star. In Table 2 we list the average infrared photometric properties of field L dwarfs, and

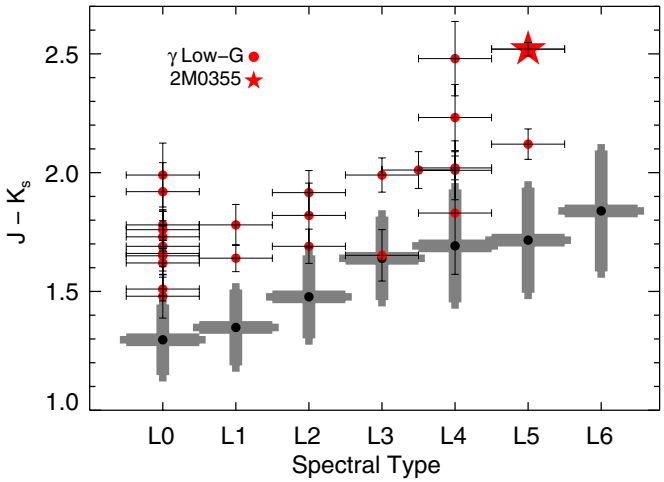

Figure 1. 2MASS ($J - K_s$) color vs. spectral type for field L dwarfs. Mean colors of normal (excluding subdwarfs, young, and low surface gravity) objects are displayed as gray bars and listed in Table 2. Only sources with *J* or *K* uncertainties <0.1 are used. Low surface gravity Lγ dwarfs are red filled circles and are listed in Tables 3 and 4. 2M0355 is marked as a five-point star.
(A color version of this figure is available in the online journal.)

in Tables 3 and 4 we list the infrared photometry and colors of low-gravity L dwarfs, respectively.

With a $J - K_s$ color of 2.52 ± 0.03, 2M0355 is 0.8 mag redder than the average for L5 dwarfs, or nearly 4σ from the mean color. A similar deviation from the mean of the subtype is seen among other low surface gravity Lγ dwarfs listed in Tables 3 and 4, but 2M0355 is the most extreme example (although we note that the L4 dwarf 2MASS J1615+4953 shows very similar deviations in both its $J - K_s$ and $W1 - W2$ colors). As discussed above, low surface gravity effects leading to a reduction in H_2 CIA are the likely cause for the extreme deviation. However we note that not all unusually red L dwarfs demonstrate low surface gravity spectral features; therefore this peculiarity alone is not conclusive about age (e.g., Looper et al. 2008).

In the same manner as Figure 1 we compile *Wide-field Infrared Survey Explorer* (*WISE*) photometry of known field L dwarfs with photometric uncertainties <0.1, excluding subdwarfs and confirmed young objects, to calculate the mean $W1 - W2$ color and corresponding standard deviation for spectral subtypes (again binned by 0.5 subtype) and highlight the photometry of 2M0355 (see also Table 2). As demonstrated in Figure 2, with a $W1 - W2$ color of 0.59, 2M0355 is 0.24 mag redder than the average of its spectral subtype or 3σ from the mean color. Comparing with the 25 similarly classified Lγ dwarfs,

[9] The compiled list of L dwarfs comes primarily from the DwarfArchives.org (http://spider.ipac.caltech.edu/staff/davy/ARCHIVE/index.shtml) combined with the results of Schmidt et al. (2010).

Table 2
Average Near-infrared and Mid-infrared Colors of L Dwarfs

SpT (1)	N_{WISE}[a] (2)	N_{2MASS}[a] (3)	N_{Low-G} (4)	$(J-K_s)_{avg}$ (5)	$\sigma(J-K_s)$ (6)	$(W1-W2)_{avg}$ (7)	$\sigma(W1-W2)$ (8)
L0	143	102	11	1.30	0.15	0.27	0.06
L1	125	95	2	1.35	0.16	0.26	0.06
L2	58	60	3	1.48	0.17	0.28	0.07
L3	69	51	3	1.64	0.18	0.31	0.06
L4	37	33	5	1.69	0.24	0.34	0.08
L5	43	28	2	1.72	0.22	0.35	0.08
L6	25	13	0	1.84	0.25	0.42	0.11
L7	13	9	0	1.75	0.26	0.46	0.09
L8-9	19	10	0	1.85	0.17	0.54	0.08

Note.
[a] Only normal (non-low surface gravity, subdwarf, or young) L dwarfs with photometric uncertainty <0.1 were used in calculating the average.

Table 3
Photometric Properties of Low Surface Gravity Lγ Dwarfs

Name (1)	SpT (OpT) (2)	J[a] (3)	H[a] (4)	K_s[a] (5)	$W1$[a] (6)	$W2$[a] (7)	$W3$[a] (8)	$W4$[a] (9)	Ref. (10)
2MASS J003255.84−440505.8	L0.0γ	14.78 ± 0.03	13.86 ± 0.03	13.27 ± 0.04	12.82 ± 0.03	12.49 ± 0.03	11.73 ± 0.19	9.29 ± null	1,2
2MASS J003743.06−584622.9	L0.0γ	15.37 ± 0.05	14.26 ± 0.05	13.59 ± 0.04	13.13 ± 0.03	12.74 ± 0.03	12.56 ± 0.38	9.32 ± null	1,2
2MASS J012445.99−574537.9	L0.0γ	16.31 ± 0.10	15.06 ± 0.09	14.32 ± 0.09	13.77 ± 0.03	13.34 ± 0.03	12.45 ± 0.31	8.91 ± null	1,2
2MASS J014158.23−463357.4	L0.0γ	14.83 ± 0.04	13.88 ± 0.02	13.10 ± 0.03	12.55 ± 0.02	12.17 ± 0.02	11.92 ± 0.21	9.24 ± null	3,2
2MASS J022354.64−581506.7	L0.0γ	15.07 ± 0.05	14.00 ± 0.04	13.42 ± 0.04	12.82 ± 0.02	12.43 ± 0.02	11.64 ± 0.15	9.47 ± null	1,2
2MASS J023400.93−644206.8	L0.0γ	15.33 ± 0.06	14.44 ± 0.06	13.85 ± 0.07	13.25 ± 0.03	12.91 ± 0.03	12.62 ± 0.28	9.49 ± null	4
2MASS J024111.51−032658.7	L0.0γ	15.80 ± 0.06	14.81 ± 0.05	14.04 ± 0.05	13.64 ± 0.03	13.26 ± 0.03	12.77 ± 0.42	9.00 ± null	2,5
2MASS J032310.02−463123.7	L0.0γ	15.39 ± 0.07	14.32 ± 0.06	13.70 ± 0.05	13.08 ± 0.02	12.67 ± 0.02	11.94 ± 0.16	9.18 ± null	1,2
2MASS J040626.77−381210.2	L0.0γ	16.77 ± 0.13	15.71 ± 0.10	15.11 ± 0.12	14.45 ± 0.03	14.10 ± 0.04	12.52 ± null	9.10 ± null	4
2MASS J195647.00−754227.0	L0.0γ	16.15 ± 0.10	15.04 ± 0.10	14.23 ± 0.07	13.69 ± 0.03	13.25 ± 0.03	12.68 ± null	9.17 ± null	1,2
2MASS J221344.91−213607.9	L0.0γ	15.38 ± 0.03	14.40 ± 0.06	13.76 ± 0.04	13.23 ± 0.03	12.83 ± 0.03	11.55 ± 0.20	9.07 ± null	2,5
2MASS J000402.88−641035.8	L1.0γ	15.79 ± 0.07	14.83 ± 0.07	14.01 ± 0.05	13.37 ± 0.03	12.94 ± 0.03	12.18 ± 0.24	9.16 ± null	4
2MASS J051846.16−275645.7	L1.0γ	15.26 ± 0.04	14.30 ± 0.05	13.62 ± 0.04	13.05 ± 0.02	12.66 ± 0.03	12.58 ± 0.35	9.22 ± null	5,6
2MASS J030320.42−731230.0	L2.0γ	16.14 ± 0.11	15.10 ± 0.09	14.32 ± 0.08	13.78 ± 0.03	13.35 ± 0.03	12.29 ± 0.17	9.34 ± 0.34	4
2MASS J053619.98−192039.6	L2.0γ	15.77 ± 0.07	14.69 ± 0.07	13.85 ± 0.06	13.26 ± 0.03	12.79 ± 0.03	12.55 ± 0.40	9.24 ± null	5,6
2MASS J232252.99−615127.5	L2.0γ	15.55 ± 0.06	14.54 ± 0.06	13.86 ± 0.04	13.24 ± 0.03	12.84 ± 0.03	12.68 ± 0.39	9.38 ± null	1,2
2MASS J172600.07+153819.0	L3.5γ	15.67 ± 0.06	14.47 ± 0.05	13.66 ± 0.05	13.07 ± 0.03	12.69 ± 0.03	11.56 ± 0.16	9.31 ± null	2,7
2MASS J212650.40−814029.3	L3.0γ	15.54 ± 0.06	14.41 ± 0.05	13.55 ± 0.04	12.91 ± 0.02	12.47 ± 0.02	11.89 ± 0.16	9.36 ± null	1,2
2MASS J220813.63+292121.5	L3.0γ	15.80 ± 0.08	14.79 ± 0.07	14.15 ± 0.07	13.35 ± 0.03	12.89 ± 0.03	12.58 ± 0.39	9.30 ± null	2,7
2MASS J012621.09+142805.7	L4.0γ	17.11 ± 0.21	16.17 ± 0.22	15.28 ± 0.15	14.24 ± 0.03	13.70 ± 0.04	12.38 ± null	9.13 ± null	6,8
2MASS J050124.06−001045.2	L4.0γ	14.98 ± 0.04	13.71 ± 0.03	12.96 ± 0.03	12.05 ± 0.02	11.52 ± 0.02	10.95 ± 0.11	9.17 ± null	1,2
2MASS J155152.37+094114.8	L4.0γ	16.32 ± 0.11	15.11 ± 0.07	14.31 ± 0.06	13.60 ± 0.03	13.12 ± 0.03	12.68 ± 0.48	9.16 ± null	1,6
2MASS J161542.55+495321.1	L4.0γ	16.79 ± 0.14	15.33 ± 0.10	14.31 ± 0.07	13.20 ± 0.02	12.62 ± 0.02	12.13 ± 0.13	9.31 ± null	5,6
2MASS J224953.45+004404.6	L4.0γ	16.59 ± 0.12	15.42 ± 0.11	14.36 ± 0.07	13.58 ± 0.03	13.14 ± 0.05	11.28 ± null	7.69 ± null	6,9,10,11
2MASS J035523.37+113343.7	L5.0γ	14.05 ± 0.02	12.53 ± 0.03	11.53 ± 0.02	10.53 ± 0.02	9.94 ± 0.02	9.29 ± 0.04	8.32 ± null	1,2
2MASS J042107.18−630602.2	L5.0γ	15.57 ± 0.05	14.28 ± 0.04	13.45 ± 0.04	12.56 ± 0.02	12.14 ± 0.02	11.60 ± 0.10	9.25 ± null	2,5

Note.
[a] JHK_s photometry from the Two Micron All Sky Catalog (Skrutskie et al. 2006) and the $W1$, $W2$, $W3$, $W4$ from *WISE* (Wright et al. 2010).
References. (1) Reid et al. 2008; (2) Cruz et al. 2009; (3) Kirkpatrick et al. 2006; (4) Kirkpatrick et al. 2010; (5) Cruz et al. 2007; (6) K. L. Cruz et al., in preparation; (7) Kirkpatrick et al. 2000; (8) Metchev et al. 2008; (9) Geballe et al. 2002; (10) Hawley et al. 2002; (11) Nakajima et al. 2004.

we find that 2M0355 is the reddest known isolated L dwarf in near- and mid-infrared colors.

4.2. Spectral Features

2M0355 is classified as an L5γ in the optical by Cruz et al. (2009) based on its similarity to field L5's but with very weak FeH absorption and weak Na I and K I lines, which are typically interpreted as signatures of low surface gravity. In Figure 3 we show the SpeX prism spectrum for 2M0355 and compare it to the field L5 (presumed age >1 Gyr) near-infrared standard 2MASS J08350622+1953050 (2M0835) as well as the ∼10 Myr L dwarf 2M1207b (Chiu et al. 2006; Kirkpatrick et al. 2010; Patience et al. 2012). We normalize the spectra separately in each bandpass and smooth 2M1207b by a factor of three. The shape of 2M0355 in all three bands deviates significantly from the spectrum of the field standard. Compared to 2M1207b, the H and K bands are very similar, but the J band is intriguingly different. 2M0355 has a steeper slope from 1.1 to 1.25 μm and a wider peak at 1.30 μm that is more similar to the field object. In a forthcoming paper, we will present a detailed J-band spectral analysis of 2M0355 and other young brown dwarfs compared to their field counterparts.

Several near-infrared spectral features are sensitive to surface gravity, including the H band where a sharp triangular peak is seen consistently for known young brown dwarfs at a range

Table 4
Colors of Low Surface Gravity Lγ Dwarfs

Name 2MASS (1)	SpT OpT (2)	$(J-K_s)$ 2MASS (3)	$(W1-W2)$ *WISE* (4)	$\Delta_{(J-K_s)}$[a] (5)	$\Delta_{(W1-W2)}$[a] (6)
2MASS J0032−4405	L0.0γ	1.51 ± 0.05	0.33 ± 0.04	0.21	0.06
2MASS J0037−5846	L0.0γ	1.78 ± 0.06	0.39 ± 0.04	0.48	0.12
2MASS J0124−5745	L0.0γ	1.99 ± 0.13	0.43 ± 0.04	0.69	0.16
2MASS J0141−4633	L0.0γ	1.73 ± 0.05	0.38 ± 0.03	0.43	0.11
2MASS J0223−5815	L0.0γ	1.65 ± 0.06	0.39 ± 0.03	0.35	0.12
2MASS J0234−6442	L0.0γ	1.48 ± 0.09	0.34 ± 0.04	0.18	0.07
2MASS J0241−0326	L0.0γ	1.76 ± 0.08	0.38 ± 0.04	0.46	0.11
2MASS J0323−4631	L0.0γ	1.69 ± 0.09	0.41 ± 0.03	0.39	0.14
2MASS J0406−3812	L0.0γ	1.66 ± 0.18	0.35 ± 0.05	0.36	0.08
2MASS J1956−7542	L0.0γ	1.92 ± 0.12	0.44 ± 0.04	0.62	0.17
2MASS J2213−2136	L0.0γ	1.62 ± 0.05	0.40 ± 0.04	0.32	0.13
2MASS J0004−6410	L1.0γ	1.78 ± 0.09	0.43 ± 0.04	0.43	0.17
2MASS J0518−2756	L1.0γ	1.64 ± 0.06	0.39 ± 0.04	0.29	0.13
2MASS J0303−7312	L2.0γ	1.82 ± 0.14	0.43 ± 0.04	0.34	0.15
2MASS J0536−1920	L2.0γ	1.92 ± 0.09	0.47 ± 0.04	0.44	0.19
2MASS J2322−6151	L2.0γ	1.69 ± 0.07	0.40 ± 0.04	0.21	0.12
2MASS J1726+1538	L3.5γ	2.01 ± 0.08	0.38 ± 0.04	0.37	0.07
2MASS J2126−8140	L3.0γ	1.99 ± 0.07	0.44 ± 0.03	0.35	0.13
2MASS J2208+2921	L3.0γ	1.65 ± 0.11	0.47 ± 0.04	0.01	0.16
2MASS J0126+1428	L4.0γ	1.83 ± 0.26	0.54 ± 0.05	0.14	0.20
2MASS J0501−0010	L4.0γ	2.02 ± 0.05	0.53 ± 0.03	0.33	0.19
2MASS J1551+0941	L4.0γ	2.01 ± 0.12	0.48 ± 0.04	0.32	0.14
2MASS J1615+4953	L4.0γ	2.48 ± 0.16	0.58 ± 0.03	0.79	0.24
2MASS J2249+0044	L4.0γ	2.23 ± 0.14	0.43 ± 0.06	0.54	0.09
2MASS J0355+1133	L5.0γ	2.52 ± 0.03	0.59 ± 0.03	0.80	0.24
2MASS J0421−6306	L5.0γ	2.12 ± 0.06	0.42 ± 0.03	0.40	0.07

Note.
[a] Δ values are calculated from the mean colors listed in Table 2.

of ages (e.g., Lucas et al. 2001; Luhman et al. 2004; Allers et al. 2007; Rice et al. 2010, 2011). In Figure 4, we present higher-resolution ($R \sim 1200$) H-band spectra of 2M0355 as well as the same comparative objects shown in Figure 3. There is an excellent match between the sharp peak of 2M1207b and 2M0355, distinct from the plateau at ∼1.55–1.70 μm of the field object. Combined with the photometric peculiarities, this is a strong indicator that 2M0355 is significantly younger than the field object (≪1 Gyr).

4.3. Kinematics

Using multi-epoch ISPI data (see Figure 5), we report improved proper motion and parallax measurements for 2M0355. The proper motion was measured previously by Schmidt et al. (2007), Casewell et al. (2008), and Faherty et al. (2009). Our updated value is consistent with previous values but with 50%–60% smaller error bars. The new parallax measurement of $\pi_{abs} = 122 \pm 13$ mas[10] for 2M0355 places the L5γ dwarf at a distance of $8.2^{+1.0}_{-0.8}$ pc. We list all astrometric and photometric properties in Table 5.

4.4. Moving Group Membership

At a distance of 8.2 pc and with spectral and photometric differences from the field population resembling those of the ∼10 Myr 2M1207b, we investigate whether 2M0355 could be kinematically associated with one of the nearby young moving groups. Using the proper motion and parallax measured in this work with the most recent RV from Blake et al. (2010), we calculate $(U, V, W) = (-5.9 \pm 1.5, -23.6 \pm 2.0, -14.6 \pm 1.3)$ km s^{-1} for 2M0355.[11] These calculated space velocities are consistent with thin disk membership (age < ∼2–3 Gyr), and the tangential velocity of 21.5 ± 1.2 km s^{-1} is consistent with the population of low gravity, kinematically young brown dwarfs (Faherty et al. 2009, 2012; Eggen 1989; Eggen & Iben 1989). In Figure 6 we show the UV velocities for a number of young stars or clusters within 200 pc of the Sun and find that 2M0355 is at the edge of a well-populated region of velocity space. Figure 7 shows Galactic space velocities compared to β Pictoris, and AB Doradus, the two closest moving groups to the Sun and the most likely groups of which 2M0355 might be a member. We find that 2M0355 overlaps within 1σ of the range in UVW values for probable members of AB Doradus.

To examine the likelihood of 2M0355's membership in nearby moving groups, we determine the χ^2 probability for several known stellar groups within 75 pc. We include a field star model and nearby moving group parameters from Malo et al. (2012) and supplement with the parameters for the Ursa Major, Hyades, and Carina Near groups. For most groups, we adopt the centroid positions and dispersions calculated by Malo et al. (2012); however, we use velocity estimates either calculated by us or from the recent literature, where we split the uncertainties in the centroid velocities from their one-dimensional (1D) intrinsic velocity dispersions.[12]

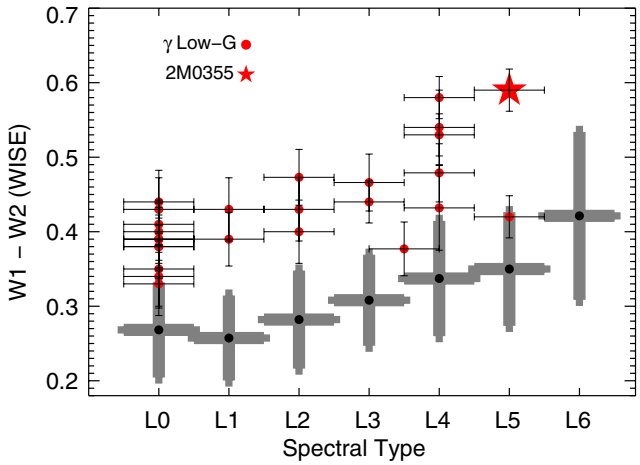

Figure 2. *WISE* $(W1 - W2)$ color vs. spectral type for field L dwarfs. Mean colors of normal (excluding subdwarfs, young, and low surface gravity) objects are displayed as gray bars and listed in Table 2. Only sources with $W1$ or $W2$ uncertainties <0.1 are used. Low surface gravity $L\gamma$ dwarfs are red filled circles and are listed in Tables 3 and 4. 2M0355 is marked as a five-point star.
(A color version of this figure is available in the online journal.)

[10] We measure $\pi_{rel} = 120 \pm 12$ mas with a 2 mas correction from relative to absolute astrometry.

[11] UVW values are calculated in a left-handed coordinate system with U positive toward the Galactic center.

[12] We adopt the following parameters throughout the analysis (centroid velocities and standard errors, followed by centroid positions and 1σ dispersions): Ursa Major: $(U, V, W) = (15.0, 2.8, -8.1) \pm (0.4, 0.7, 1.0)$ km s^{-1} and $(X, Y, Z) = (-4.4, 6.2, 18.2) \pm (16.7, 15.4, 17.0)$ pc (calculated using membership from Madsen et al. 2002). Carina Near: $(U, V, W) = (-24.8, -18.2, -2.3) \pm (0.7, 0.7, 0.4)$ km s^{-1} and $(X, Y, Z) = (0.1, -31.7, -9.2) \pm (4.3, 5.6, 1.1)$ pc (calculated using membership from Zuckerman et al. 2006). Hyades: $(U, V, W) = (-42.3, -19.1, -1.5) \pm (0.1, 0.1, 0.2)$ km s^{-1} and $(X, Y, Z) = (-43.0, 0.3, -17.3) \pm (3.8, 3.5, 3.1)$ pc. For the TWA group we adopt the recent centroid velocity from Weinberger et al. (2011) of $(U, V, W) = (-11.1, -18.6, -5.1) \pm (0.3, 0.2, 0.2)$ km s^{-1}. Based on unpublished calculations by Mamajek (2010) and E. E. Mamajek (in preparation), we adopt intrinsic 1D velocity dispersions of 1.0 km s^{-1} for AB Doradus, 1.1 km s^{-1} for Tucana–Horologium, 1.3 km s^{-1} for Carina Near, 1.5 km s^{-1} for Ursa Majoris, and β Pictoris, 0.8 km s^{-1} for TWA (Mamajek 2005), and 1 km s^{-1} for the Hyades and Argus.

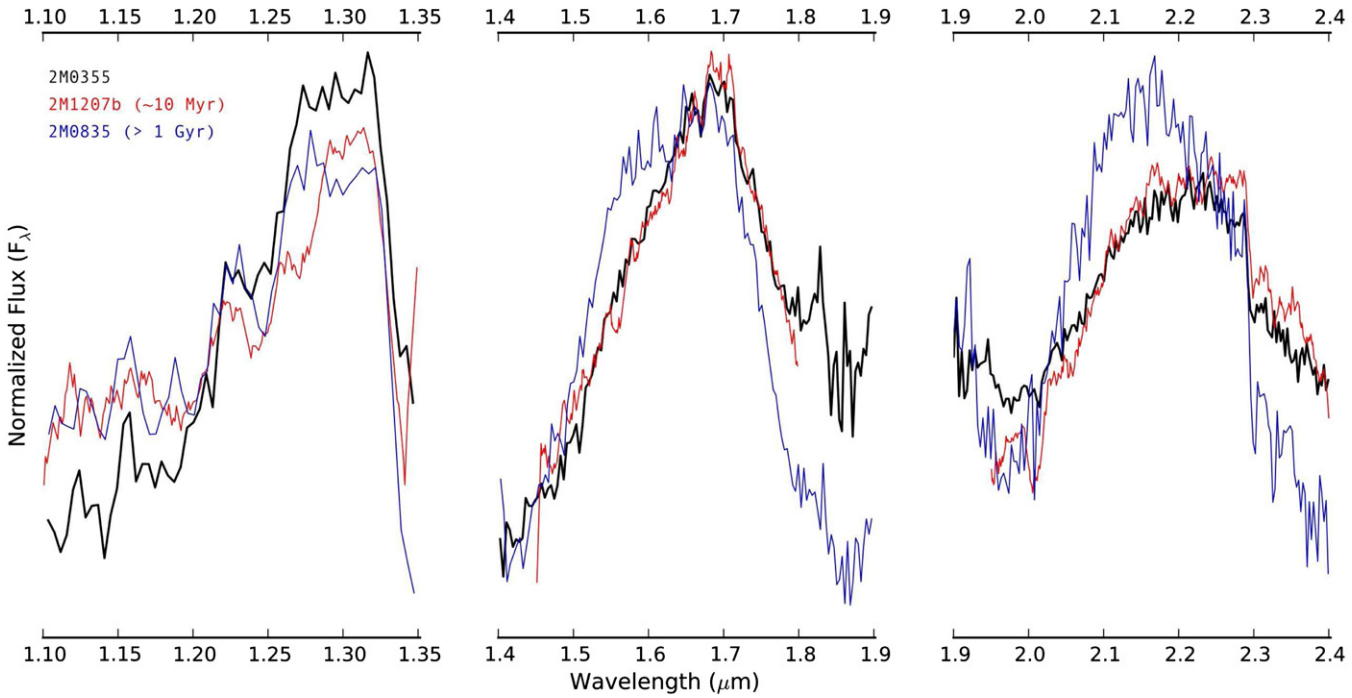

Figure 3. SpeX prism near-infrared spectra of 2M0355 (black solid line) compared to the L5 near-infrared standard (blue dashed line) 2M0835 (defined in Kirkpatrick et al. 2010) and the young planetary-mass companion (red dashed line) 2M1207b (from Patience et al. 2010). We separate *JHK* bands and normalize the three objects over each band independently. 2M0355 deviates from the field L5 with a sharply peaked *H* band and suppressed *K* band, and matches well with the features of 2M1207b.

(A color version of this figure is available in the online journal.)

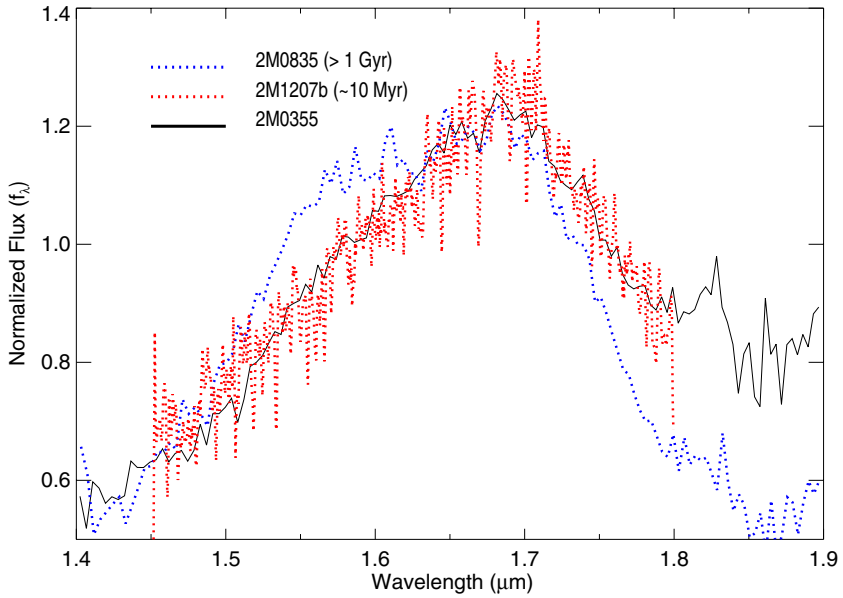

Figure 4. SpeX cross-dispersed *H*-band spectra of 2M0355 (black solid line) compared to the field L5 near-infrared standard (blue dashed line) 2M0835 (defined in Kirkpatrick et al. 2010) and the young planetary-mass companion (red dashed line) 2M1207b (from Patience et al. 2012). The strong triangular shape seen in 2M1207b and 2M0355 is interpreted as a hallmark of low surface gravity.

(A color version of this figure is available in the online journal.)

We first determine a χ^2 probability that estimates the percentage of real members of a given group expected to have χ^2 values higher than that of 2M0355—allowing for 2M0355's observational errors and the estimated intrinsic velocity spread and spatial distribution of group members. Then we calculate a "final" probability, normalizing by the sum of the individual (marginal) star-group probabilities. At this time, equal weights are assigned to the field star and individual group models (further refinement would be beyond the focus of this study).

The initial χ^2 probability for six degrees of freedom is calculated as

$$\chi^2 = A + B \quad (1)$$

$$A = \frac{(U_o - U_g)^2}{\sigma_U^2} + \frac{(V_o - V_g)^2}{\sigma_V^2} + \frac{(W_o - W_g)^2}{\sigma_W^2} \quad (2)$$

$$\sigma_i = \sqrt{\sigma_{i,o}^2 + \sigma_{i,g}^2 + \sigma_{i,d}^2}, \quad (3)$$

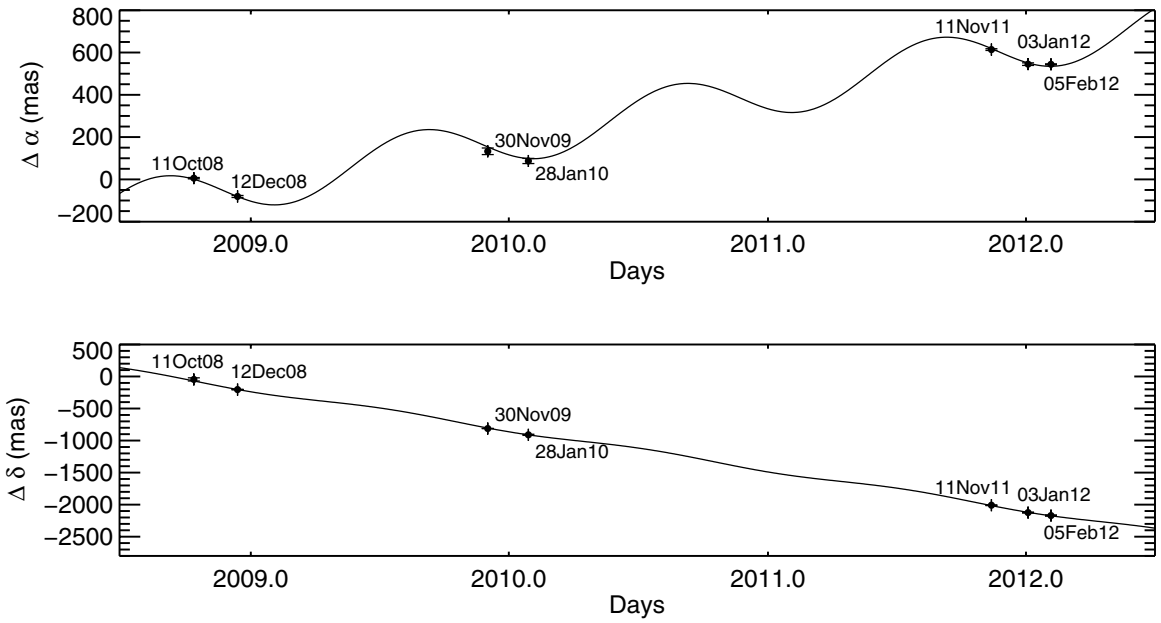

Figure 5. ISPI astrometry for 2M0355. The upper panel shows the imaging results (filled points) as well as the best-fit solution for the proper and parallactic motion in right ascension and the lower panel shows the same in declination.

Table 5
Properties of 2MASS J035523.37+113343.7

Parameter	Value	Reference
(1)	(2)	(3)
R.A., decl. (J2000)	$03^h55^m23\overset{s}{.}37$ +11°33′43″.7	1
Optical SpT	L5γ	2
J (2MASS)	14.05 ± 0.02	1
H (2MASS)	12.53 ± 0.03	1
K_s (2MASS)	11.53 ± 0.02	1
J (MKO)[a]	13.90 ± 0.03	4
H (MKO)[a]	12.60 ± 0.03	4
K (MKO)[a]	11.46 ± 0.02	4
M_J (MKO)	14.33 ± 0.24	4
M_H (MKO)	13.03 ± 0.24	4
M_K (MKO)	11.89 ± 0.23	4
$W1$	10.53 ± 0.02	3
$W2$	9.94 ± 0.02	3
$W3$	9.29 ± 0.04	3
$W4$	8.32 ± null	3
μ_α	218 ± 5 mas yr^{-1}	4
μ_δ	−626 ± 5 mas yr^{-1}	4
π_{abs}	122 ± 13 mas	4
RV	11.92 ± 0.22 km s^{-1}	5
U[b]	−5.9 ± 1.5 km s^{-1}	4
V[b]	−23.6 ± 2.0 km s^{-1}	4
W[b]	−14.6 ± 1.3 km s^{-1}	4
X[b]	−7.0 ± 0.7 pc	4
Y[b]	0.2 ± 0.4 pc	4
Z[b]	−4.2 ± 0.4 pc	4
Age[c]	50–150 Myr	4
Mass[c]	13–30 M_{Jup}	4

Notes.
[a] MKO values calculated using the transformations in Stephens & Leggett (2004).
[b] UVW and XYZ values are calculated in a left-handed coordinate system with U and X positive toward the Galactic center.
[c] Age and mass are based on the fact that we estimate a 43% probability that 2M0355 is an AB Doradus member.
References. (1) Cutri et al. 2003; (2) Cruz et al. 2009; (3) Wright et al. 2010; (4) This paper; (5) Blake et al. 2010.

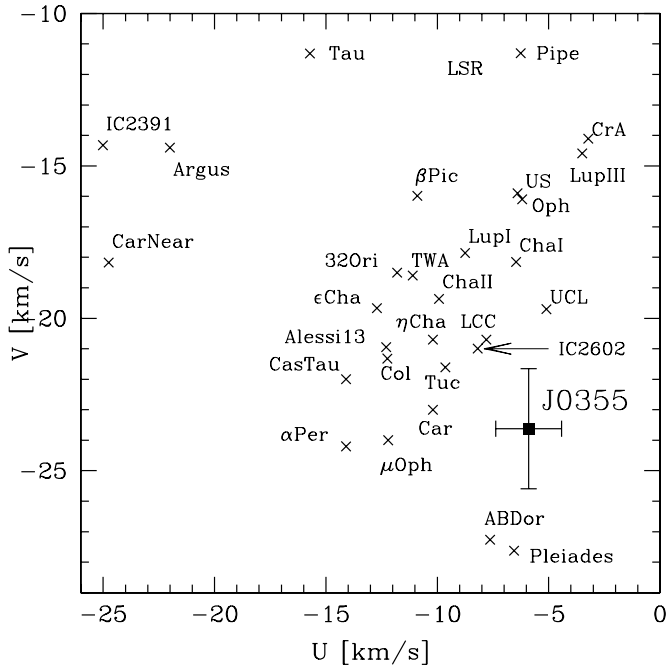

Figure 6. U vs. V velocity plot for a large collection of young stellar groups within 200 pc of the Sun from Mamajek (2010). 2M0355 is highlighted as a filled square and is located in a busy region of velocity space for nearby young objects.

where i is indexed as U, V, or W, o is the component for 2M0355, g is the component of the group, and d is the intrinsic 1D i-velocity dispersion of the group:

$$B = \frac{(X_o - X_g)^2}{\Delta_X^2} + \frac{(Y_o - Y_g)^2}{\Delta_Y^2} + \frac{(Z_o - Z_g)^2}{\Delta_Z^2} \quad (4)$$

$$\Delta_j = \sqrt{\Delta_{j,o}^2 + \Delta_{j,g}^2}, \quad (5)$$

where j is indexed as X, Y, or Z, Δ_j is defined as the 1σ dispersion in the Galactic Cartesian coordinates, o is the

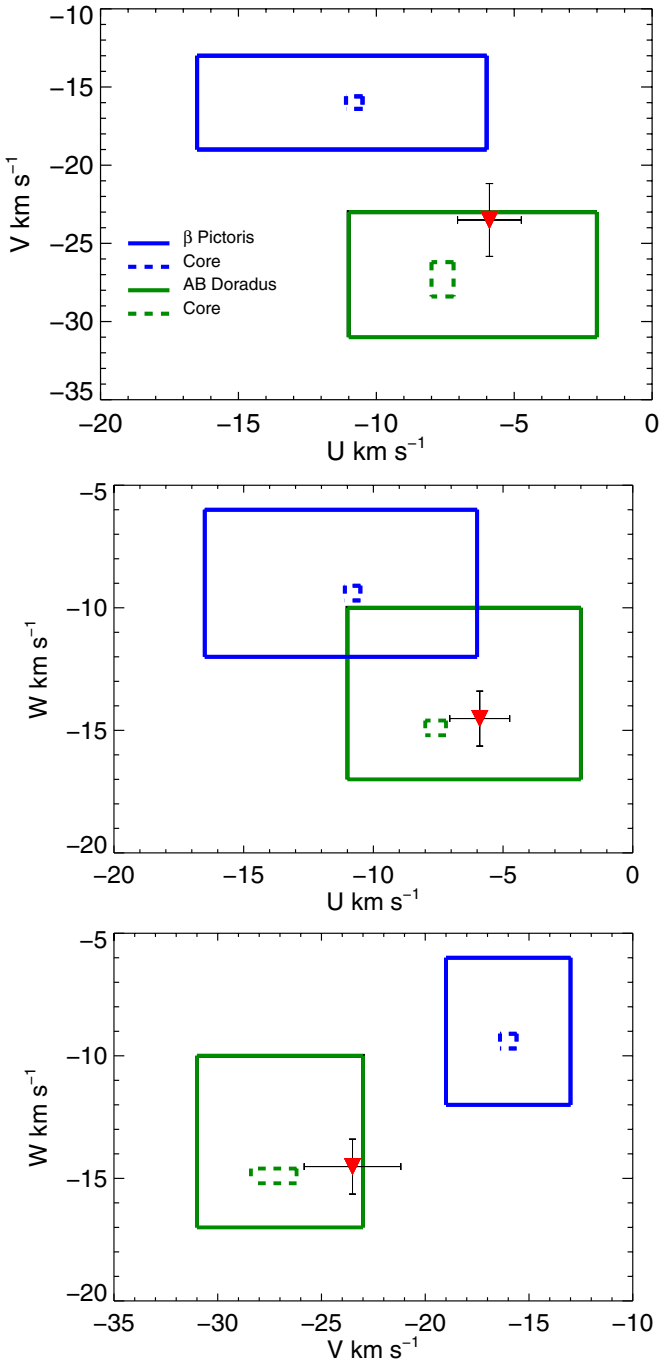

Figure 7. *UVW* properties of 2M0355 (red filled triangle) compared to those of the members of the nearby young groups β Pictoris (blue) and AB Doradus (green). Solid rectangles surround the furthest extent of highly probable members from Torres et al. (2008) but their distribution does not necessarily fill the entire rectangle. We also show the core *UVW* values of β Pictoris (-10.9 ± 0.3, -16.0 ± 0.3, -9.2 ± 0.3) km s^{-1} and AB Doradus (-7.6 ± 0.4, -27.3 ± 1.1, -14.9 ± 0.3) km s^{-1} from Mamajek (2010) updated using the revised *Hipparcos* astrometry from van Leeuwen (2007) and the compiled velocity catalog of Gontcharov (2006).

(A color version of this figure is available in the online journal.)

component for 2M0355, and g is the component for the group (we ignore the uncertainties in the group centroids which are negligible compared to the 1σ dispersions).

Using this method, we estimate that 73% of AB Doradus members would have velocities and positions more discrepant than that for 2M0355, while only 0.06% of β Pictoris members

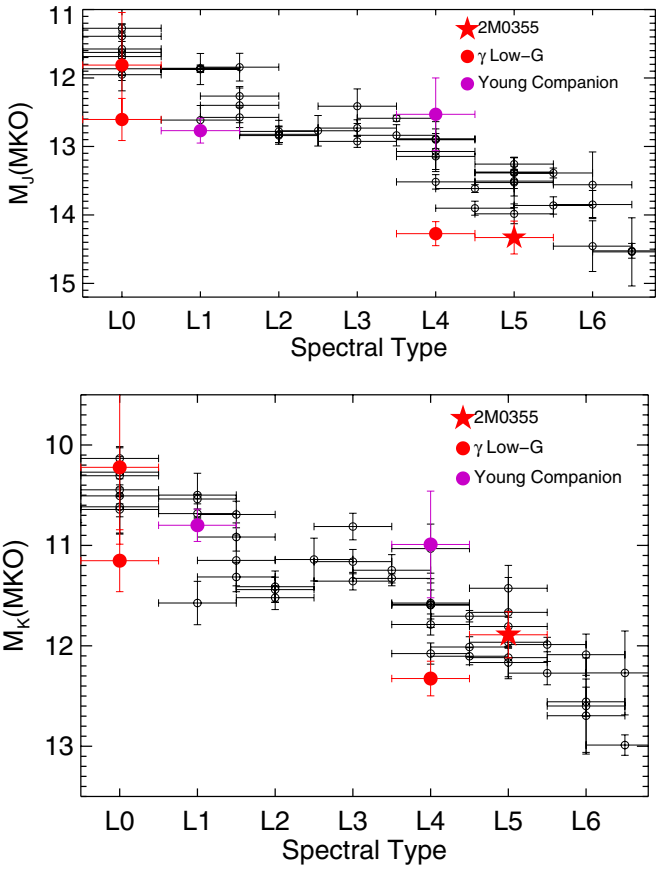

Figure 8. Spectral type vs. absolute magnitude diagram in MKO J (top) and K (bottom) for L dwarfs. Normal objects (non-binary, young, or subdwarf) are shown as open black circles, Lγ dwarfs as filled red circles, and young companion brown dwarfs as filled purple circles. 2M0355 is highlighted as a red five-point star.

(A color version of this figure is available in the online journal.)

would have more discrepant values. Approximately 99.9% of field stars would have velocities and positions more discrepant than that of 2M0355, although this is likely skewed by the fact that the field star centroid (as well as our source) is so close to the Sun.

The χ^2 probabilities for the other groups investigated within 75 pc (Ursa Majoris, Carina Near, Tucana–Horologium, Hyades, Argus, TWA), all yielded probabilities of $<10^{-17}$%. If one sums the individual marginal group and field star membership probabilities and assigns equal weights, then we estimate that 2M0355 has a 42% chance of being an AB Doradus member, a 58% chance of being a field star, and a <0.04% chance of being a β Pictoris group member. Further work calculating the relative densities of the young stellar groups could refine these probabilities, but at this point it appears most plausible that 2M0355 is either a member of the AB Doradus moving group or a field star. Given the photometric and spectroscopic evidence for youth shown herein combined with the low density of very young field stars, we believe that the kinematic evidence points toward 2M0355 being a likely member of the AB Doradus group.

5. DISCUSSION

Among the known population of low surface gravity L dwarfs, 2M0355+11 is the latest spectral type or one of the coolest isolated young brown dwarfs known. To extend the comparison of

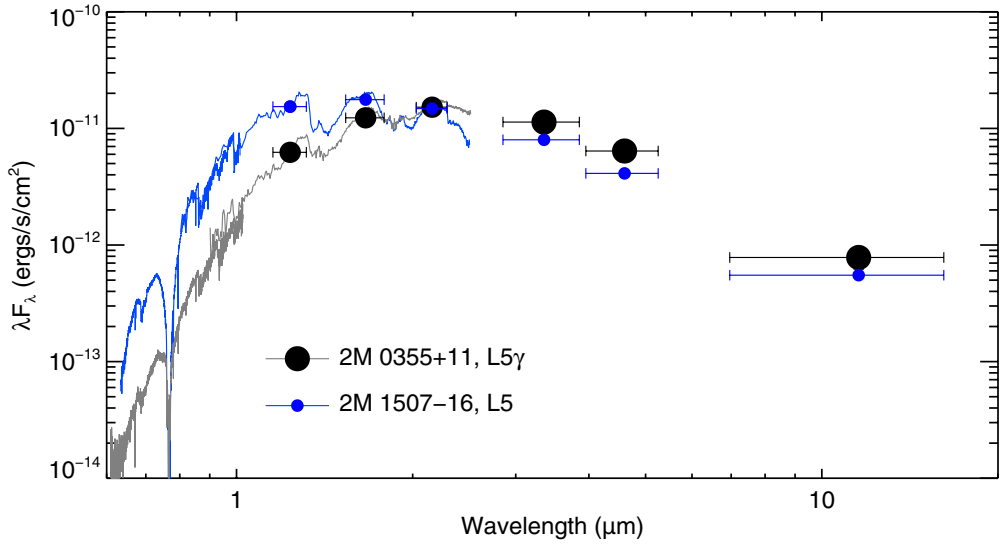

Figure 9. Optical spectra, 2MASS *JHK*, and *WISE* $W1$, $W2$, $W3$, $W4$ photometry of 2M0355 (gray spectra and black filled circles) compared to the field L5 2M1507 (blue spectra and filled points). The absolute photometry calculated from the parallax of each object (this work; Dahn et al. 2002) as well as flux-calibrated optical spectra scaled to the near-IR photometry are transformed into λF_λ. 2M0355 is underluminous through K and then overluminous through $\sim$12 μm.
(A color version of this figure is available in the online journal.)

young brown dwarfs and planetary-mass objects, we investigate the colors and luminosities of 2M1207b and the directly imaged planets HR 8799bcd.

We calculated the absolute magnitude of 2M0355 from the new parallax as well as Mauna Kea Observatory (MKO; Tokunaga et al. 2002) apparent magnitudes converted from 2MASS photometry using the Stephens & Leggett (2004) relations. Comparing M_{JHK} for 2M0355 to the predicted values for an equivalent spectral type object based on the Faherty et al. (2012) polynomial, we find it to be [−0.9,−0.5,−0.1] mag underluminous at M_J, M_H, and M_K, respectively. As noted in Faherty et al. (2012), the population of low surface gravity L dwarfs is consistently red and underluminous—by up to 1.0 mag in M_{JHK}—compared to equivalent spectral type objects. As demonstrated in Figure 8, 2M0355 clearly follows this trend. As discussed in Faherty et al. (2012) evolutionary models trace low surface gravity objects at temperatures several hundred degrees lower than expected for equivalent spectral type objects on near-IR color–magnitude diagrams, providing a potential explanation for the deviation in absolute magnitudes of low-gravity L dwarfs. Extending this analysis to 2M0355 we conclude that one explanation for its peculiar near-IR absolute magnitudes is that this source is cooler than normal L5 field dwarfs.

In Figure 9 we compare the full SED of 2M0355 to the field L5 dwarf 2MASS J1507476−162738 (2M1507; Reid et al. 2000; Dahn et al. 2002). Combining the optical spectra, MKO *JHK*, and *WISE* $W1$, $W2$, $W3$ absolute photometry for each we confirm that the SED for 2M0355 is underluminous compared to the field object through K band. However, redward of $\sim$2.5 μm, 2M0355 switches to being overluminous through at least 12 μm. Following the method described in Cushing et al. (2005), we combine the flux-calibrated optical and near-IR spectra as well as *WISE* photometry and calculate bolometric luminosities for both 2M0355 and 2M1507. We linearly interpolate between the centers of each *WISE* bandpass ($W1$: 3.4; $W2$: 4.6; $W3$: 11.6) and assume a Rayleigh–Jeans tail for $\lambda > 11.6$ μm. We find that 2M0355 is slightly more luminous than 2M1507 by $\Delta \log_{10}(L_{2M0355}/L_{2M1507}) = 0.12 \pm 0.1$. The overall luminosity of our source is further evidence that it is young, and we surmise that enhanced photospheric dust which weakens molecular bands and shifts flux to longer wavelengths is the most likely cause of the red SED.

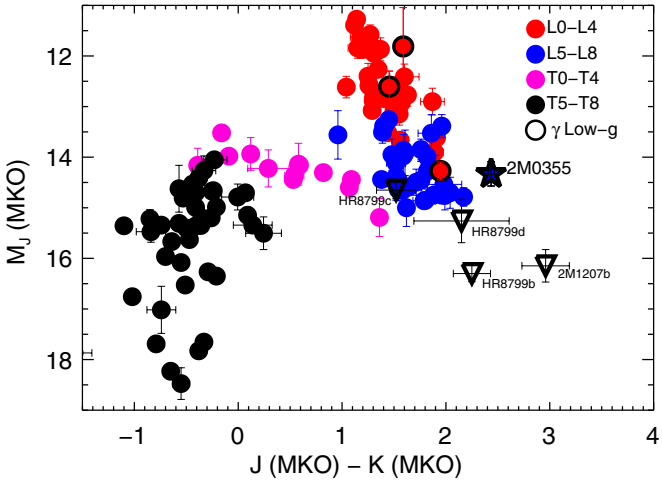

Figure 10. Near-infrared color–magnitude diagram for field and low surface gravity Lγ brown dwarfs as well as giant planetary-mass companions. Absolute magnitudes were derived from parallaxes reported in Faherty et al. (2012) and Dupuy & Liu (2012). We highlight the location of 2M0355 and note that it occupies a similar region of color–magnitude space as 2M1207b and HR8799b.
(A color version of this figure is available in the online journal.)

In Figure 10 we show the near-infrared color–magnitude diagram for the field brown dwarf population (color-coded by spectral type), 2M1207b, the HR8799bcd planets, and 2M0355. The low luminosity and extremely red $J-K$ color of 2M0355 place it at the red edge of the brown dwarf population, in a similar region as 2M1207b. Barman et al. (2011) find the positions of the giant exoplanets on this color–magnitude diagram—which are also redward and underluminous of the brown dwarf population—can be reproduced by allowing low $T_{\rm eff}$ models (typically assumed cloud-free) to have clouds extending across their photospheres (see also Bowler et al. 2010; Currie et al. 2011; Hinz et al. 2010; Marley et al. 2012;

Madhusudhan et al. 2011; Skemer et al. 2012). 2M1207b and HR8799bcd are young (∼10 Myr and 30–160 Myr, respectively; Chauvin et al. 2004; Marois et al. 2008, 2010) so youth is thought to be correlated with enhanced photospheric dust among the low-luminosity, low-temperature brown dwarfs and giant exoplanets (see also Burgasser et al. 2010; Faherty et al. 2012).

Consequently, the position of 2M0355 in Figure 10 leads us to conclude that in agreement with indications from the SED in Figure 9 this source is both young and dusty.

6. CONCLUSIONS

2M0355 is the reddest isolated L dwarfs yet characterized in the near- and mid-infrared. Cruz et al. (2009) classified 2M0355 as L5γ, indicating low surface gravity spectral signatures. The similarity of the near-infrared spectrum to that of the ∼10 Myr planetary-mass object 2M1207b supports the conclusion that the object is young. Furthermore, a comparison with the near- and mid-infrared colors of the known population of low surface gravity or Lγ dwarfs demonstrates that 2M0355 is the most extreme example of this class currently known.

Combining optical spectra and absolute near- to mid-IR photometry, we compared the full SED of 2M0355 with the field L5 dwarf 2M1507−16. We find that 2M0355 is underluminous in optical through the *K* band then switches to overluminous through at least 12 μm compared to 2M1507−16. Calculating the bolometric luminosity by integrating over the optical and near-IR spectra as well as *WISE* photometry shows that the overall luminosity of 2M0355 is overluminous compared to the field object. We conclude that enhanced photospheric dust, thought to be correlated with young, low-temperature, low-luminosity brown dwarfs, and giant exoplanets, shifts flux to longer wavelengths creating the red SED. The position of 2M0355 on the near-IR color–magnitude diagram supports this conclusion as it appears redward and underluminous of the known population in a similar region as 2M1207b and HR8799bcd.

Combining new proper motion and parallax measurements, we calculate *UVW* velocities to evaluate membership in nearby young moving groups. We find that the kinematics consistent with the young thin disk and the UV velocities for 2M0355 place it in a busy part of velocity space for young objects. A careful kinematic comparison with nearby young groups and the field population leads us to conclude that 2M0355 has a 42% chance of membership in AB Doradus. 2M0355 remains the brightest isolated low surface gravity L dwarf studied to date and will prove to be a useful comparative object in low-temperature atmosphere studies directly applicable to giant exoplanets.

Despite the spectral similarity to 2M1207b in *H* and *K*, 2M0355 is substantially different from the planetary-mass object in *J* band. This, combined with the older age estimate for 2M0355, causes the temperature and mass of 2M0355 to remain ambiguous. Nevertheless, we can use the object's absolute photometry and constrained age (assuming membership in AB Doradus) to estimate these key properties. Using the evolutionary tracks for young, low-mass objects of Baraffe et al. (2002), we estimate an effective temperature of ∼1500 K and a mass of ∼13 $M_{\rm Jup}$ for an age of 50 Myr (the lower limit for the age of AB Doradus). At the upper age limit for AB Doradus, ∼150 Myr, the mass of 2M0355 would be closer to ∼30 $M_{\rm Jup}$. As a field object, the absolute magnitudes of 2M0355 correspond to an object of ∼70 $M_{\rm Jup}$, slightly below hydrogen burning minimum mass.

We acknowledge receipt of observation time through NOAO and we thank 4.0 m telescope operators C. Aguilera, M. Gonzalez, and A. Alvarez. We also thank M. Cushing and the anonymous referee for useful comments regarding the manuscript. K.C. gratefully acknowledges support from the Research Initiative for Scientific Enhancement program at Hunter College funded by the National Institute of Health. This publication has made use of the data products from the Two Micron All Sky Survey, which is a joint project of the University of Massachusetts and the Infrared Processing and Analysis Center/California Institute of Technology, funded by the National Aeronautics and Space Administration and the National Science Foundation. This research has made use of the NASA/ IPAC Infrared Science Archive, which is operated by the Jet Propulsion Laboratory, California Institute of Technology, under contract with the National Aeronautics and Space Administration. This research has benefited from the M, L, and T dwarf compendium housed at DwarfArchives.org (http://spider.ipac.caltech.edu/staff/davy/ARCHIVE/index.shtml) and maintained by Chris Gelino, Davy Kirkpatrick, and Adam Burgasser. This research has made use of NASA's Astrophysics Data System. The authors wish to recognize and acknowledge the very significant cultural role and reverence that the summit of Mauna Kea has always had within the indigenous Hawaiian community. We are most fortunate to have the opportunity to conduct observations from this mountain.

REFERENCES

Allers, K. N., Jaffe, D. T., Luhman, K. L., et al. 2007, ApJ, 657, 511
Baraffe, I., Chabrier, G., Allard, F., & Hauschildt, P. H. 2002, A&A, 382, 563
Barman, T. S., Macintosh, B., Konopacky, Q. M., & Marois, C. 2011, ApJ, 733, 65
Bernat, D., Bouchez, A. H., Ireland, M., et al. 2010, ApJ, 715, 724
Blake, C. H., Charbonneau, D., & White, R. J. 2010, ApJ, 723, 684
Blake, C. H., Charbonneau, D., White, R. J., Marley, M. S., & Saumon, D. 2007, ApJ, 666, 1198
Boss, A. P., Weinberger, A. J., Anglada-Escudé, G., et al. 2009, PASP, 121, 1218
Bowler, B. P., Liu, M. C., Dupuy, T. J., & Cushing, M. C. 2010, ApJ, 723, 850
Burgasser, A. J. 2004, ApJL, 614, L73
Burgasser, A. J., Cruz, K. L., & Kirkpatrick, J. D. 2007, ApJ, 657, 494
Burgasser, A. J., Kirkpatrick, J. D., Brown, M. E., et al. 2002, ApJ, 564, 421
Burgasser, A. J., Kirkpatrick, J. D., Burrows, A., et al. 2003, ApJ, 592, 1186
Burgasser, A. J., Simcoe, R. A., Bochanski, J. J., et al. 2010, ApJ, 725, 1405
Burrows, A., Hubbard, W. B., Lunine, J. I., & Liebert, J. 2001, RvMP, 73, 719
Burrows, A., Marley, M., Hubbard, W. B., et al. 1997, ApJ, 491, 856
Casewell, S. L., Jameson, R. F., & Burleigh, M. R. 2008, MNRAS, 390, 1517
Chabrier, G., & Baraffe, I. 1997, A&A, 327, 1039
Chabrier, G., Baraffe, I., Allard, F., & Hauschildt, P. 2000, ApJ, 542, 464
Chauvin, G., Lagrange, A.-M., Dumas, C., et al. 2004, A&A, 425, L29
Chiu, K., Fan, X., Leggett, S. K., et al. 2006, AJ, 131, 2722
Cruz, K. L., Kirkpatrick, J. D., & Burgasser, A. J. 2009, AJ, 137, 3345
Cruz, K. L., Reid, I. N., Kirkpatrick, J. D., et al. 2007, AJ, 133, 439
Currie, T., Burrows, A., Itoh, Y., et al. 2011, ApJ, 729, 128
Cushing, M. C., Kirkpatrick, J. D., Gelino, C. R., et al. 2011, ApJ, 743, 50
Cushing, M. C., Looper, D., Burgasser, A. J., et al. 2009, ApJ, 696, 986
Cushing, M. C., Rayner, J. T., & Vacca, W. D. 2005, ApJ, 623, 1115
Cushing, M. C., Vacca, W. D., & Rayner, J. T. 2004, PASP, 116, 362
Cutri, R. M., Skrutskie, M. F., van Dyk, S., et al. 2003, 2MASS All-sky Catalog of Point Sources, VizieR Online Data Catalog
Dahn, C. C., Harris, H. C., Vrba, F. J., et al. 2002, AJ, 124, 1170
Dhital, S., West, A. A., Stassun, K. G., & Bochanski, J. J. 2010, AJ, 139, 2566
Dupuy, T. J., & Liu, M. C. 2012, ApJS, 201, 19
Eggen, O. J. 1989, PASP, 101, 54
Eggen, O. J., & Iben, I. J. 1989, AJ, 97, 431
Faherty, J. K., Burgasser, A. J., Cruz, K. L., et al. 2009, AJ, 137, 1
Faherty, J. K., Burgasser, A. J., Walter, F. M., et al. 2012, ApJ, 752, 56
Faherty, J. K., Burgasser, A. J., West, A. A., et al. 2010, AJ, 139, 176
Geballe, T. R., Knapp, G. R., Leggett, S. K., et al. 2002, ApJ, 564, 466
Gizis, J. E., Faherty, J. K., Liu, M. C., et al. 2012, AJ, 144, 94

Gontcharov, G. A. 2006, A&AT, 25, 145
Gorlova, N. I., Meyer, M. R., Rieke, G. H., & Liebert, J. 2003, ApJ, 593, 1074
Hawley, S. L., Covey, K. R., Knapp, G. R., et al. 2002, AJ, 123, 3409
Hinz, P. M., Rodigas, T. J., Kenworthy, M. A., et al. 2010, ApJ, 716, 417
Kirkpatrick, J. D. 2005, ARA&A, 43, 195
Kirkpatrick, J. D., Barman, T. S., Burgasser, A. J., et al. 2006, ApJ, 639, 1120
Kirkpatrick, J. D., Looper, D. L., Burgasser, A. J., et al. 2010, ApJS, 190, 100
Kirkpatrick, J. D., Reid, I. N., Liebert, J., et al. 1999, ApJ, 519, 802
Kirkpatrick, J. D., Reid, I. N., Liebert, J., et al. 2000, AJ, 120, 447
Knapp, G. R., Leggett, S. K., Fan, X., et al. 2004, AJ, 127, 3553
Looper, D. L., Kirkpatrick, J. D., Cutri, R. M., et al. 2008, ApJ, 686, 528
Lucas, P. W., Roche, P. F., Allard, F., & Hauschildt, P. H. 2001, MNRAS, 326, 695
Luhman, K. L., Peterson, D. E., & Megeath, S. T. 2004, ApJ, 617, 565
Madhusudhan, N., Burrows, A., & Currie, T. 2011, ApJ, 737, 34
Madsen, S., Dravins, D., & Lindegren, L. 2002, A&A, 381, 446
Malo, L., Doyon, R., Lafrenière, D., et al. 2012, AJ, in press (arXiv:1209.2077)
Mamajek, E. E. 2005, in Proc. Conf. Protostars and Planets V (Houston, TX: LPI), http://www.lpi.usra.edu/meetings/ppv2005/pdf/8522.pdf, 8522
Mamajek, E. E. 2010, BAAS, 42, 473
Marley, M. S., Saumon, D., Cushing, M., et al. 2012, ApJ, 754, 135
Marois, C., Macintosh, B., Barman, T., et al. 2008, Sci, 322, 1348
Marois, C., Zuckerman, B., Konopacky, Q. M., Macintosh, B., & Barman, T. 2010, Natur, 468, 1080
McGovern, M. R., Kirkpatrick, J. D., McLean, I. S., et al. 2004, ApJ, 600, 1020
Metchev, S. A., Kirkpatrick, J. D., Berriman, G. B., & Looper, D. 2008, ApJ, 676, 1281
Mohanty, S., Jayawardhana, R., Huélamo, N., & Mamajek, E. 2007, ApJ, 657, 1064
Nakajima, T., Tsuji, T., & Yanagisawa, K. 2004, ApJ, 607, 499
Patience, J., King, R. R., de Rosa, R. J., & Marois, C. 2010, A&A, 517, A76
Patience, J., King, R. R., De Rosa, R. J., et al. 2012, A&A, 540, A85
Radigan, J., Jayawardhana, R., Lafrenière, D., et al. 2012, ApJ, 750, 105
Rayner, J. T., Toomey, D. W., Onaka, P. M., et al. 2003, PASP, 115, 362
Reid, I. N., Cruz, K. L., Kirkpatrick, J. D., et al. 2008, AJ, 136, 1290
Reid, I. N., Kirkpatrick, J. D., Gizis, J. E., et al. 2000, AJ, 119, 369
Reid, I. N., Lewitus, E., Allen, P. R., Cruz, K. L., & Burgasser, A. J. 2006, AJ, 132, 891
Rice, E. L., Faherty, J. K., Cruz, K., et al. 2011, in ASP Conf. Ser. 448, 16th Cambridge Workshop on Cool Stars, Stellar Systems, and the Sun, ed. C. Johns-Krull, M. K. Browning, & A. A. West (San Francisco, CA: ASP), 481
Rice, E. L., Faherty, J. K., & Cruz, K. L. 2010, ApJL, 715, L165
Saumon, D., Hubbard, W. B., Burrows, A., et al. 1996, ApJ, 460, 993
Schmidt, S. J., Cruz, K. L., Bongiorno, B. J., Liebert, J., & Reid, I. N. 2007, AJ, 133, 2258
Schmidt, S. J., West, A. A., Hawley, S. L., & Pineda, J. S. 2010, AJ, 139, 1808
Skemer, A. J., Hinz, P. M., Esposito, S., et al. 2012, ApJ, 753, 14
Skrutskie, M. F., Cutri, R. M., Stiening, R., et al. 2006, AJ, 131, 1163
Stephens, D. C., & Leggett, S. K. 2004, PASP, 116, 9
Tinney, C. G., Faherty, J. K., Kirkpatrick, J. D., et al. 2012, ApJ, 759, 60
Tokunaga, A. T., Simons, D. A., & Vacca, W. D. 2002, PASP, 114, 180
Torres, C. A. O., Quast, G. R., Melo, C. H. F., & Sterzik, M. F. 2008, in Handbook of Star Forming Regtons, Vol. II: The Southern Sky, ed. B. Reipurth (San Francisco, CA: ASP), 757
Vacca, W. D., Cushing, M. C., & Rayner, J. T. 2003, PASP, 115, 389
van der Bliek, N. S., Norman, D., Blum, R. D., et al. 2004, Proc. SPIE, 5492, 1582
van Leeuwen, F. 2007, A&A, 474, 653
Weinberg, M. D., Shapiro, S. L., & Wasserman, I. 1987, ApJ, 312, 367
Weinberger, A. J., Anglada-Escudé, G., & Boss, A. 2011, BAAS, 43, 2011
Wright, E. L., Eisenhardt, P. R. M., Mainzer, A. K., et al. 2010, AJ, 140, 1868
Zuckerman, B., Bessell, M. S., Song, I., & Kim, S. 2006, ApJL, 649, L115